
PLATOON FUNDAMENTAL DIAGRAM ESTIMATION CAN BE MARKOVIAN: EVIDENCE FROM HUMAN- AND SELF-DRIVEN VEHICLE TRAJECTORIES

A PREPRINT

Michail A. Makridis

IVT, Civil Environmental and Geomatic Engineering
ETH Zurich, Switzerland
mmakridis@ethz.ch

Anastasios Kouvelas

IVT, Civil Environmental and Geomatic Engineering
ETH Zurich, Switzerland
kouvelas@ethz.ch

Jorge A. Laval

Civil and Environmental Engineering
Georgia Institute of Technology, US
jorge.laval@ce.gatech.edu

January 31, 2024

ABSTRACT

We propose a simple and effective method to derive the Fundamental Diagram (FD) from platoon vehicle trajectories. Average traffic state variables are computed using Edie's generalized definitions within time-dependent trapezoidal space-time areas. To obtain a clear FD, we employ a bivariate data aggregation technique to eliminate scatter. Our findings are as follows: (i) The proposed method demonstrates a remarkably consistent relation between the traffic variables and a clear triangular shape for autonomously-driven vehicles. (ii) The FDs are invariant to several factors of heterogeneity such as the platoon length, vehicle characteristics, road particularities, and data acquisition accuracy. (iii) ACC-driven vehicle platoons with minimum headway setting achieve much higher capacity, roughly 90% than those with a large headway setting. (iv) Connectivity might increase capacity. (v) Human drivers have a wider near-capacity operation area, showing different behaviors at high speeds than low ones, and (vi) Safety concerns might arise due to high values of backward wave speed for ACC-driven vehicles. Comparative analysis with the state-of-the-art confirms the validity of our approach. The proposed method stands out due to its simplicity and accuracy, which paves the way for practical applications in real-time traffic flow monitoring and control within modern intelligent transportation systems.

1 Introduction

Traffic investigations, initiated nearly 90 years ago, aimed to better comprehend the intricate phenomena occurring in road transport systems. Among early pioneers was Greenshields who in 1933 noticed a linear relation between speed and traffic density and a parabolic relation between speed and traffic flow using the assumption that traffic flow equals traffic density multiplied by speed, also known as Fundamental Diagram (FD). Since then, numerous studies in the literature exploit the concept of FD as a congestion modeling tool for traffic estimation purposes at link or network levels [Kouvelas et al. \(2017\)](#); [Makridis and Kouvelas \(2023\)](#); [Du et al. \(2023\)](#).

The study of vehicle platoon trajectories has been ongoing for over 50 years. In 1966, [Treiterer \(1975\)](#) used aerial photographs from a helicopter, following a specific vehicle and monitoring the traffic around it, as all vehicles progress along the roadway. Subsequently, [Treiterer and Myers \(1974\)](#) observed a generally retarded behavior displayed by a platoon of vehicles after emerging from a kinematic disturbance as compared to the behavior of the same vehicles

approaching the disturbance, known today as traffic hysteresis phenomenon. This discovery sparked a continued interest in platoon dynamics.

The exploration of platoon trajectories is appealing due to its ability to offer insights into the behavior of different drivers under similar conditions, which directly influences traffic state. The existence of diverse driver behaviors on public roads has been widely recognized as a catalyst for various traffic phenomena. Consequently, there is a strong interest in accurately modeling and simulating this heterogeneity, as discussed in [Makridis et al. \(2020a\)](#). Moreover, the integration of automation and connectivity in vehicles further amplifies the impact of drivers' behaviors on road capacity and utilization [Ioannou \(1997\)](#); [van Arem et al. \(2006\)](#); [Makridis et al. \(2020d\)](#). However, there is limited information in the existing literature regarding how different driver modes may contribute to distinct Fundamental Diagrams (FDs).

Fortunately, a growing number of experimental datasets that include human-driven and automated vehicles emerge, as in [Makridis et al. \(2021\)](#); [Gunter et al. \(2021\)](#). Such datasets provide valuable opportunities to gain fresh insights into the topic. While there is extended research on the microscopic properties of partially or fully automated vehicles such as reaction time [Brunner et al. \(2022\)](#); [Makridis et al. \(2020c\)](#), string instability [Li et al. \(2021\)](#); [Gunter et al. \(2021\)](#), safety [Lu et al. \(2021\)](#); [Mattas et al. \(2020\)](#); [Mullakkal-Babu et al. \(2020\)](#), and energy efficiency [Apostolakis et al. \(2023\)](#); [He et al. \(2020\)](#); [Ma et al. \(2021\)](#), there are very few works that explicitly relate their microscopic behavior with the traffic state. Although there are some recent efforts, see [Chen et al. \(2017\)](#); [Shi and Li \(2021\)](#), achieving generalization is not a straightforward task due to challenges from various factors such as road geometry, platoon length, diverse vehicle specifications, or data acquisition frequency. This paper takes advantage of the operational properties of commercial ACC (and CACC) systems to aim for a constant headway policy. It proposes a simple and robust numerical method to describe macroscopic traffic flow properties of ACC- and CACC-driven platoons of vehicles.

By analyzing observations from either fully or partially automated vehicles and applying an aggregation technique, we establish a clear relationship between the three traffic flow variables: speed, density, and flow. This results in clear FD for homogeneous drivers in platoons, using only inexpensive raw trajectory observations. Due to the absence of ground-truth information, the validity of the method in terms of traffic state inference is assessed using one of the currently most reliable methods for traffic state inference in the literature [Laval \(2011\)](#); [Maiti et al. \(2023\)](#), and the resemblance is remarkably high.

Our method proves to be robust against heterogeneity from means of observations, including variations in noise levels, platoon synthesis, platoon length, and traffic conditions. Additionally, it eliminates the need for estimating the backward wave speed and minimizes computational complexity. The results reveal a triangular shape for the FD of partially automated vehicles and provide concrete insights into the expected capacity and speed-dependent dynamic behavior of human drivers compared to partially automated vehicles. At the same time, safety concerns arise for ACC-driven vehicles with minimum distance settings.

In the remainder of this paper, we present in Section 2 the proposed methodology, while Section 3 discusses the results and finally, conclusions are summarized in Section 4.

2 Methodology

First, we adopt the well-known Edie's generalized definitions for raw movement data aggregation to derive fundamental traffic variables, namely, flow, density, and space-mean speed, see [Edie \(1965\)](#); [Cassidy and Coifman \(1997\)](#).

It is important to note that in this procedure, a rectangular area needs to be defined, and the flow, density, and speed are calculated based on the number of vehicle-kilometers traveled and vehicle-time traveled within this region. Based on the most acknowledged measurement method in the literature, see [Laval \(2011\)](#), the shape of this region should be a sided rectangle including the platoon vehicles with side slopes representing the expected backward wave speed. This approach is crucial to avoid blending different traffic states and to obtain a reliable approximation of the prevailing traffic state within the given space-time area. However, implementation-wise there are numerical difficulties for discrete observations. Additionally, defining a global representation of the fundamental diagram (FD) for a driver mode remains an unresolved matter, particularly when analyzing large trajectory datasets due to the significant variability observed.

In this study, we first attempt to estimate the traffic state at a given time based on two consecutive observations. The data resolution (usually $10Hz$) does not affect the final results. Through this process, the estimated traffic states are derived, which are equal in number to the total number of observations minus one.

Here, we present an example that illustrates how to determine the effective platoon length, which establishes the boundaries of our designated area. Figure 1a depicts a platoon of vehicles with their antennas used for data acquisition. The observed platoon length represents the distance between the first and last antenna, excluding a portion of the first

and last vehicle. Assuming equal vehicle lengths and identical antenna positions on each vehicle, this corresponds to the distance between the back bumper of the leader and the back bumper of the last follower. To account for assumptions' variability and measurement noise, we incorporate a small buffer space (approximately 3 meters). This adjusted length is referred to as the effective platoon length, which varies dynamically as the vehicles move. Figure 1b provides a schematic representation of the area used for the computation of speed, density, and flow. For the mathematical representation, we refer the reader to A.

The computation of the instantaneous traffic states described above is carried out for all available datasets, classified according to the driver mode (human, ACC with fixed distance setting, and CACC). This generates a large number of potential states and a significant amount of scatter. We aim to verify if all the observations that correspond to the same driver mode, e.g., ACC with the minimum setting, correspond to the same fundamental diagram. To derive a single fundamental diagram (FD) relationship, we employ a simple and efficient data aggregation technique across all available data.

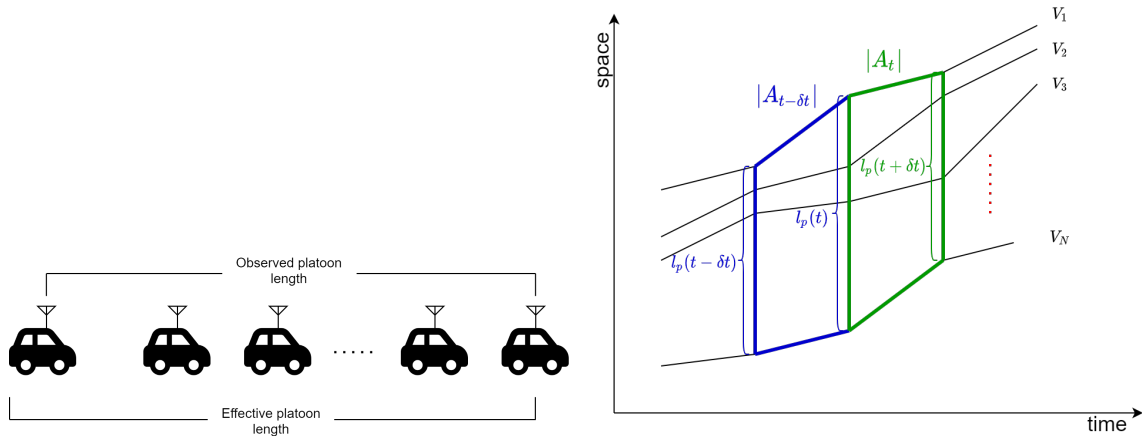
In the flow-density representation, we divide the observed density range into bins of length δ_k . Within each density interval, we calculate the average of all observed flow values, yielding a single estimated flow value per density bin. An exemplary illustration is given in Figure 2. As expected, the accuracy of the fundamental traffic state improves with more observations. The results show that the inferred fundamental traffic states per driver mode are independent of the bin length, δ_k . A similar aggregation process is applied to the observed speed range with aggregation of observed flow values within each speed interval. The aggregation is applied to the density and speed ranges since we expect a concave flow function over each of these quantities. The aggregation process is formally described in A.

3 Results

The method we propose is implemented using data gathered from nine independent campaigns and across five driver modes for platooning. These clusters consist of ACC-driven vehicles with minimum, median, and maximum settings, cooperative ACC-driven vehicles, and human drivers. Although the number of observations for ACC-driven vehicles with minimum and maximum settings is significantly higher than for the other clusters, we present results incorporating all available data. Further information regarding the data used can be found in B and the relevant literature.

Figure 3 illustrates the flow-density plot of the FD for two methods, the observed driver modes and a $\delta_k = \delta_v = 0.3$. Please note that despite the absence of traffic state ground-truth, we compare the proposed method with Laval (2011) as a benchmark technique and we verify the realistic traffic state inference. The inferred FDs with the proposed method (Figure 3a) and the existing state-of-the-art in the literature (Figure 3b) are very similar. The results for the other two bi-level plots, namely Speed-Density and Flow-Speed are provided in C.

The black lines in Figure 3a correspond to the triangular fundamental diagram (TFD) that was calibrated on the data from ACC-driven vehicles with a minimum and maximum setting (two driver modes with available observations). Calibration was performed with minimization of the sum of normalized root mean square errors of the flow and speed. Further information on the calibration process can be found in D.



(a) Illustration of the observed and effective platoon length. (b) Illustration of moving scalene trapezoid space-time area.

Figure 1: Schematic representation of an observed platoon and a dynamic area for instantaneous traffic state estimation.

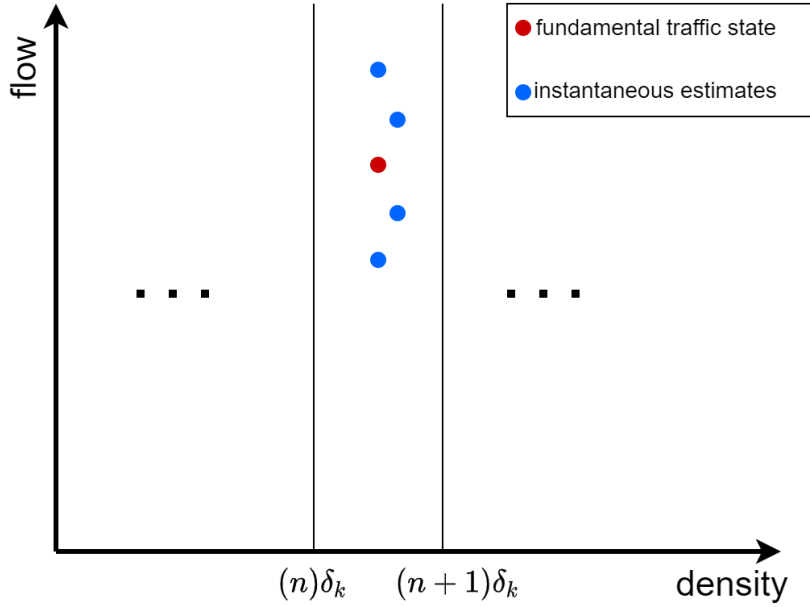


Figure 2: Schematic representation of the aggregation method. Blue dots correspond to instantaneous traffic state estimates for the same driver mode. Each dot corresponds to an observation without considering the experiment, platoon size, powertrain, etc. All estimates have instantaneous density within the bin range, i.e., $k \in (n\delta_k, (n+1)\delta_k)$. The inferred fundamental traffic state for the corresponding bin is derived by averaging all observed instantaneous densities. Therefore each density bin corresponds to one flow value.

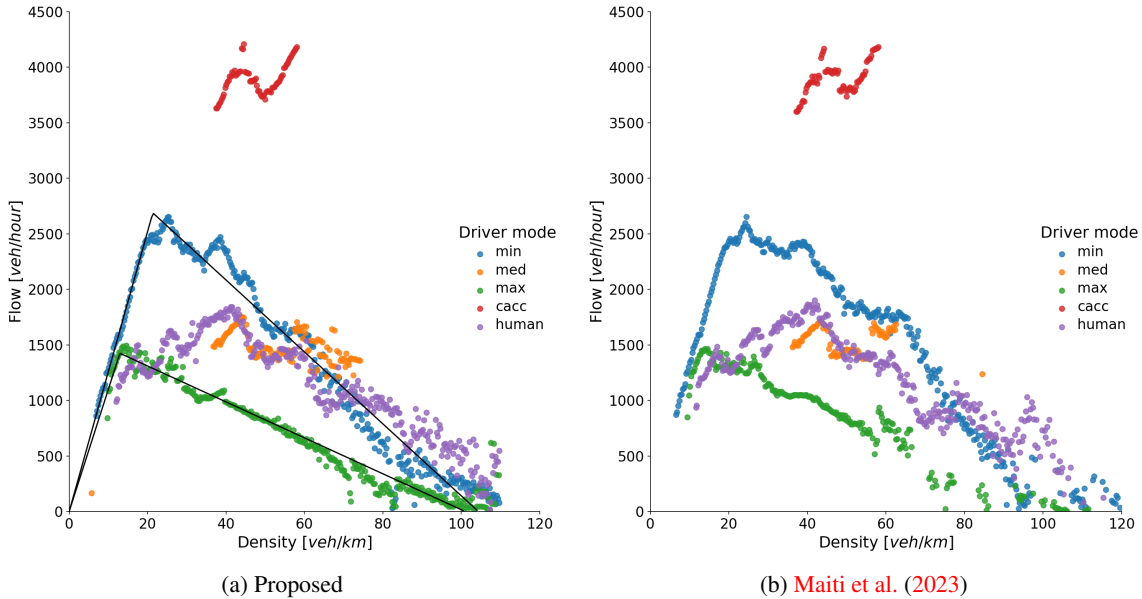


Figure 3: Flow-Density plot with the proposed method and the measurement method proposed by [Laval \(2011\)](#) after the application of the Shear transformation described in [Maiti et al. \(2023\)](#) and the aggregation process described in this paper.

The calibrated inferred FDs exhibit remarkable consistency with the TFD shape. However, depending on the aggregation strength (defined by δ), some TFD parameters might lose their significance during calibration when there is insufficient available data. For instance, the observed speeds for the maximum ACC setting only range up to 120 [km/h], while for the minimum ACC setting, they reach 140 [km/h], see [Figure 5a](#) and [5b](#). As a result, the calibration of the free-flow

part for the former might not be accurate. Similarly, it is currently not meaningful to provide calibrated TFD for the other driver modes, namely, medium ACC setting and CACC, due to scarcity of data.

Another interesting observation relates to the calibrated backward wave speed values for the ACC-driven vehicles that are given in Table 2. ACC-driven vehicles with maximum setting have realistic wave speed of around 15-17km/h. However, the same variable for ACC-driven vehicles with minimum setting has been found to be over 30km/h. This reveals safety concerns for such platoons. An in-depth investigation is out of the present paper’s scope but will be part of future research.

While the available data for human drivers may seem sufficient, it appears that the TFD shape only poorly describes their behavior. The respective FD has a more smooth shape with a very wide near-capacity area. The behavioral analysis of the FD for human drivers reveals commonalities and differences between human behavior and control behavior which eventually is also reflected in traffic flow. By referring to Figure 5 (provided in C), it can be observed that human drivers behave similarly to ACC-driven vehicles with a maximum setting at higher speeds (above 50 [km/h]). However at lower speeds (below 30 [km/h]), reflecting congested conditions, human drivers take greater safety risks by maintaining much shorter distances from vehicles ahead. Consequently, their behavior aligns more closely with ACC-driven vehicles with a minimum setting. In terms of traffic implications, such behavior leads to better road utilization compared to partially automated vehicles under over-saturated conditions nearing jam density. Unfortunately, there is no available data to observe the corresponding behavior of CACC-driven vehicles but it would be interesting to explore this in future research. Finally, the above analysis conceptually aligns with empirical evidence, showing human drivers being more relaxed at higher speeds, allowing for larger time gaps, while being more agile at lower speeds to minimize their travel time, see Xu et al. (2021).

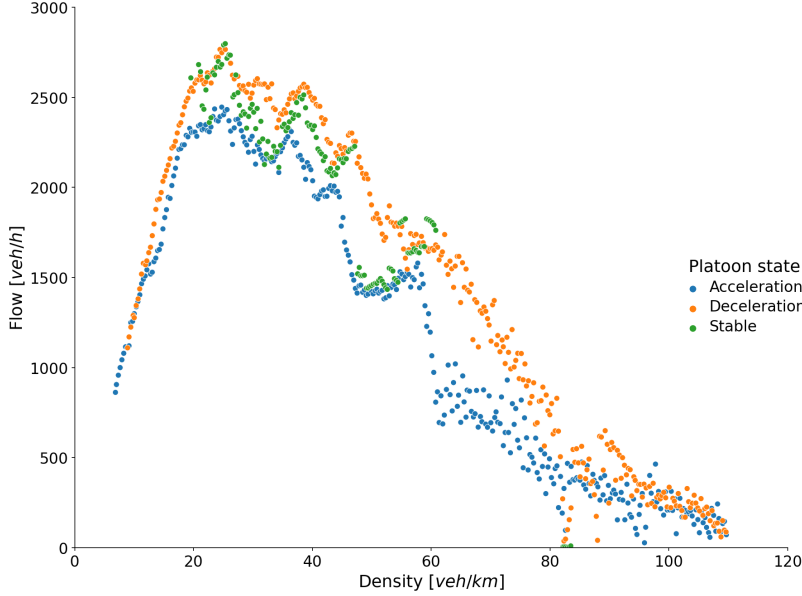
Consistent with existing literature, the findings presented in this study suggest that connectivity in ACC systems has the potential to improve traffic flow. Although the empirical data available is limited, it is evident that the observed behavior of CACC-driven vehicles differs significantly from both ACC-driven and human-driven vehicles. While we cannot derive precise values for capacity, critical density, and jam density due to the scarcity of data, it is evident that the potential for improvement is substantial. The observed flow reaches around 4000 [veh/h] (possibly higher overall) as can be seen in Figure 3. Furthermore, Figure 5 in Annex C shows that they manage to maintain the same platoon speed as the other modes (ACC and human drivers) under very high density, thus very close inter-vehicle spacing. This, of course, can be attributed to the effect of connectivity that provides more information to the vehicles, so that, they can keep a close distance from their leaders without compromising safety and stability. It should be noted, however, that further empirical data is necessary to validate the safety and robustness of CACC systems in the face of communication interference threats.

It is important to acknowledge that the nominal capacity values mentioned earlier assume ideal uniform driving conditions, which are not reflective of real-world environments. However, the relevant FD characteristics provide valuable insights into the variations in efficiency among different driver modes of transportation and the potential each mode holds. Such information is essential for the design and implementation of optimal traffic management and control strategies.

3.1 Analysis of different platoon states

In the literature, the estimation of stationary conditions in a platoon dataset is necessary for the inference of traffic variables as mentioned in Laval (2011). However, this is not a requirement for the proposed method. Nevertheless, during platoon acceleration, deceleration, and stable (cruising) states, different behaviors arise and therefore it is interesting to be able to observe if and how such states affect a unified FD representation. Consequently, we post-process all available data and categorize the platoon trajectories into three platoon states, namely acceleration, deceleration, and stable state events. Categorization is performed by inferring partial trajectories where the average platoon speed is increasing, decreasing, or remaining constant. The idea is then to aggregate traffic variables per platoon state so that we analyze their impact on the unified FD representation. For more in-depth information about the processing details, we refer the reader to Annex E.

The results with the proposed method per platoon state for ACC-driven vehicles with minimum setting are illustrated in Figure 4. The traffic states corresponding to stable platoon state lie between those of accelerating and decelerating states, at (visually) equal distances. Interestingly, by looking only at stable platoon states, we would not have been able to infer the complete FD.



(a) Flow-Density plot - proposed

Figure 4: Flow-Density plot for different platoon states. The plots refer to observed vehicle platoons driven with the ACC minimum setting.

3.2 Sensitivity of δ parameter in calibrated FD

The results presented so far refer to δ_k and δ_v parameters equal to $0.3 [veh/km]$ and $0.3 [km/h]$ values for data aggregation. Here we test the consistency of the calibrated TFD parameters through a sensitivity analysis for different δ values ranging from 0.3 to 3.5 density/speed units. The results validate completely the consistency of the inferred FD in all cases and they are summarized in Table 2 in F. It is interesting to observe that the calibrated TFD parameters for the minimum and maximum δ s are really close, even if higher δ leads to very few points for calibration.

4 Conclusion

We study different experimental observations with platoons of vehicles driven by five driver modes, i.e., Adaptive Cruise Control (ACC) with minimum, medium and maximum setting, Cooperative-ACC (CACC) and human drivers. We propose a numerically simple and effective method to derive the Fundamental Diagram (FD) per driver mode after the application of a bivariate aggregation technique. The proposed method demonstrates a remarkably consistent relation between the traffic variables and a clear triangular shape for autonomously-driven vehicles. Comparison with a state-of-the-art method from the literature confirms the validity of the inferred states. Two important benefits are the absence of a need to assume a backward wave speed and to estimate stationary conditions.

The driver mode with minimum ACC setting points to much higher capacity values (roughly 90%) than ACC-driven vehicles with maximum setting or human drivers. However, this also leads to much higher backward wave speed, raising safety concerns. Preliminary results with limited data show that connectivity can significantly improve capacity. The FD shape for automated vehicles is triangular, while human drivers exhibit a wider near-capacity area.

A Methodology

Eddie's generalized definition is given for reference below:

$$k = \sum_{i=1}^N t_i / |A| \quad (1a)$$

$$q = \sum_{i=1}^N x_i / |A| \quad (1b)$$

$$v = q/k = \sum_{i=1}^N x_i / \sum_{i=1}^N t_i \quad (1c)$$

where k , q and v stand for density, flow, and speed in the region: A , $|A|$ is the area of A and t_i , x_i is the travel time and distance traveled respectively, of vehicle i inside $|A|$.

The effective platoon length $l_p(t)$, is shown in Figure 1b and it is dynamic over time as the vehicles move. We define $|A|$ as a time-variant scalene trapezoid area described but two consecutive platoon steps. Such a simplification is by design particularly useful and inexpensive for the analysis of discrete trajectory observations.

Let us assume that we have platoon observations with N vehicles and a constant data acquisition frequency equal to $f = \frac{1}{\delta t}$. Figure 1b provides a schematic representation of the area used for the computation of speed, density, and flow. Considering that the platoon $l_p(t)$ at two consecutive time instances, we derive $|A|$ numerically as follows:

$$|A(t)| = \frac{l_p(t) + l_p(t + \delta t)}{2} \delta t \quad (2)$$

Speed, density, and flow variables for a platoon of N vehicles and for a fixed observation interval δt are computed accordingly:

$$k(t) = (N\delta t) / |A(t)| = 2N / (l_p(t) + l_p(t + \delta t)) \quad (3a)$$

$$q(t) = \sum_{i=1}^N \delta x_i(t) / |A(t)| \quad (3b)$$

$$v(t) = q(t)/k(t) = \sum_{i=1}^N \delta x_i(t) / (N\delta t) \quad (3c)$$

where $\delta x_i(t) = x_i(t + \delta t) - x_i(t)$, derived by the individual vehicle positions at times t and $t + \delta t$.

In the remaining part of this Appendix, we describe formally the aggregation process applied on the available observation per driver mode. Let us define a set of $M + 1$ discrete equally spaced values as follows:

$$B = \{0 * \delta, 1 * \delta, \dots, M * \delta\} \quad (4)$$

where δ is the discrete quantity interval and B is the corresponding set of discrete quantity values. In our case, we create two sets, one for density discretization and another for speed discretization, with the corresponding δ_k and δ_v intervals, i.e. $B_k = \{0 * \delta_k, 1 * \delta_k, \dots, M * \delta_k\}$ and $B_v = \{0 * \delta_v, 1 * \delta_v, \dots, M * \delta_v\}$.

In order to compute the aggregated values for $v - k$ and $q - k$ plots based on observed density, speed and flow variables, i.e. $k(t)$, $v(t)$, $q(t)$, for each δ_k within B_k , we average all available measurements across all datasets to derive $M + 1$ points that describe the central data tendency.

$$\{k, v, q\}_i = \begin{cases} \frac{1}{T_i} \sum_{t=1}^{T_i} k(t), & \text{where } i * \delta_k \leq k(t) \leq (i + 1) * \delta_k, \forall i \in \{0, \dots, M_k\} \\ \frac{1}{T_i} \sum_{t=1}^{T_i} v(t), & \text{where } i * \delta_k \leq k(t) \leq (i + 1) * \delta_k, \forall i \in \{0, \dots, M_k\} \\ \frac{1}{T_i} \sum_{t=1}^{T_i} q(t), & \text{where } i * \delta_k \leq k(t) \leq (i + 1) * \delta_k, \forall i \in \{0, \dots, M_k\} \end{cases} \quad (5)$$

where T_i refers to the total number of $k(t)$, $v(t)$, $q(t)$ measurements when $k(t)$ lies within $(i * \delta_k, (i + 1) * \delta_k]$.

Finally, for the computation of aggregated values for v - q , since it is expected a two-valued function across the flow, the aggregation is performed on the speed in a similar way as Eq. 5 with δ_v interval according to the following equation:

$$\{v, q\}_i = \begin{cases} \frac{1}{T_i} \sum_{t=1}^{T_i} v(t), & \text{where } i * \delta_v \leq v(t) \leq (i + 1) * \delta_v, \forall i \in \{0, \dots, M_v\} \\ \frac{1}{T_i} \sum_{t=1}^{T_i} q(t), & \text{where } i * \delta_v \leq v(t) \leq (i + 1) * \delta_v, \forall i \in \{0, \dots, M_v\} \end{cases} \quad (6)$$

where T_i refers to the total number of available $k(t)$, $v(t)$, $q(t)$ measurements when $v(t)$ lies within $(i * \delta_v, (i + 1) * \delta_v]$. Please note that $M_k = M_v$ in the case that $\delta_k = \delta_v$. For simplicity, in the results of this work, we use the same δ values on the density and flow axes.

B Data

The proposed methodology is demonstrated through empirical observations from car-following campaigns with platoons of vehicles. Eleven campaigns from five major datasets are considered in this work. The observations refer to human-driven, ACC-driven and CACC-driven vehicles. The total distance traveled per platoon in all experiments is 844.8 [km] for ACC-driven platoons, 38.2 [km] for human-driven platoons and 29.3 [km] for CACC-driven platoons. A brief introduction of each campaign follows while all datasets are summarized in TABLE 1.

Table 1: Summary of experimental campaigns used in this work.

	Driver	ACC settings	Number of vehicles	Homogenous
<i>AstaZero</i>	ACC:172 [km]/HV:22.9 [km]	min	5	No
<i>ZalaZone</i> (Handling)	ACC:49.5 [km]/HV:15.3 [km]	min/max	4-10	No
<i>ZalaZone</i> (Dynamic)	ACC:67.3 [km]	min/med/max	4-11	No
<i>Cherasco</i>	ACC:6.5 [km]	min	3	No
<i>Casale</i>	ACC:142.5 [km]	min	2	Yes
<i>JRC</i>	ACC:10.9 [km]	min/med	2/3	Yes/No
<i>CARMA</i>	CACC:29.3 [km]	-	5	Yes
<i>VU1</i>	ACC:390 [km]	min/max	2	Yes
<i>VU2</i>	ACC:6.1 [km]	min	7	Yes

B.0.1 OpenACC dataset

The OpenACC dataset was initiated by the open-access policy of the Joint Research Centre of the European Commission and involves a set of car-following experiments with human-driven and ACC-driven vehicles on public roads, test tracks, and the JRC private urban network. The dataset is constantly populated and this work includes campaigns that are not mentioned in the original publication. In this work, we use car-following observations from *AstaZero*, *ZalaZone*, *Cherasco*, *Casale*, and *JRC* campaigns. More details about the OpenACC can be found in [Makridis et al. \(2021\)](#). Currently, available campaigns can be downloaded from the [Makridis et al. \(2020b\)](#) website.

B.0.2 CARMA dataset

The United States Department of Transportation has developed a proof-of-concept platooning system that, additionally to the familiar ACC, includes V2V and V2I communication. This CACC implementation is based on the Cooperative Automation Research and Mobility Applications (CARMA) platform. As described in [Tiernan et al. \(2017\)](#), the first version of *CARMA* dataset was acquired in 2016 at the Aberdeen Test Center in Maryland. In this work, we use the second subsequent campaign, *CARMA2*, a platooning experiment presented in [Tiernan et al. \(2019\)](#) in 2018. The experiment included five vehicles of the same model and was conducted on the 7.2 [km] two-lane road of the proving ground. The features of the test track are assumed to be similar to the typical US highway. Spacing measurements were

obtained with PinPoint GPS, while for speed measurements the production wheel speed was used. More details on the dataset can be found in the above-mentioned reports.

B.0.3 Vanderbilt University dataset

The *Vanderbilt University dataset* includes two campaigns with car-following data of ACC-driven vehicles. During the first campaign (VU1) four speed profiles are recorded to observe the behavior of each vehicle in the two-vehicle tests. For all tests, the vehicles begin on the track and start at a low speed with a full-size sedan as the lead vehicle, and the test vehicle as the follower vehicle. To validate the emergent traffic flow behavior of ACC vehicles at the aggregate (system) level, a second campaign (VU2) was conducted where seven identical ACC vehicles follow a lead vehicle that creates a velocity slow down event. Position and speed data for each vehicle were collected using high-accuracy uBlox EVK-M8T GPS receivers. For more information we refer the reader to the corresponding publication [Gunter et al. \(2021\)](#).

C Fundamental Diagrams

The flow-density plots are given in Figure 3a and 3b. Here we provide additionally the Speed-Density and Flow-Speed plots for both methods in Figure 5. Calibrated FDs fit very nicely on the data with a minimum and maximum ACC setting. Unfortunately, there are limited data on CACC-driven vehicles but figures show great potential for increased capacity and critical density for this technology. It can safely be assumed that this result is due to the additional information from vehicle connectivity. As mentioned in Section 3, the FD for human drivers seems to be between the FD of ACC-driven vehicles with minimum setting and those with a maximum setting. Attempting to interpret this finding intuitively, we can assume that humans drive keeping larger time spaces at high speeds, while they keep shorter spacings at low speeds, i.e., the congested branch of the FD. Finally, as expected ACC-driven vehicles with a medium setting generate FD points between those with a maximum and a minimum setting.

D Calibration of the Triangular Fundamental Diagram

For calibration purposes, we use the triangular fundamental diagram (TFD) proposed by [Daganzo \(1995\)](#), which is probably the most widespread. The TFD has been chosen due to its simplicity in the implementation, describing the density-flow plane with a bi-linear relation. More specifically, the flow-density function is adequately described by the following:

$$Q(k) = \begin{cases} v_f k, & \text{if } k \leq k_{cr} \\ w(k_{jam} - k), & \text{if } k \geq k_{cr} \end{cases} \quad (7)$$

where v_f is the free-flow speed, w is the wave speed, k_{cr} is the critical density and k_{jam} is the jam density.

Based on trigonometry and assuming having critical density k_{cr} , the first and second leg of Equation 7 are equal. Therefore, we can derive the following equation for the wave speed and reduce the number of variables by one:

$$w = \frac{v_f k_{cr}}{k_{jam} - k_{cr}} \quad (8)$$

From Equations 7 and 8 we have:

$$Q(k) = \begin{cases} v_f k, & \text{if } k \leq k_{cr} \\ \frac{v_f k_{cr}}{k_{jam} - k_{cr}} k, & \text{if } k \geq k_{cr} \end{cases} \quad (9)$$

Consequently we perform the following simple optimization operation on the v - k (see Figure 3) and the parameter vector $x = [v_f, k_{cr}, k_{jam}]$, which contains the parameters of the TFD:

$$x = \arg \min_{x: lb \leq x \leq ub} Q_{\S} \quad (10)$$

where lb and ub are the lower and upper bounds for the three variables of the TFD. Q_{\S} is the objective function, based on the root mean square errors between observations and the TFD:

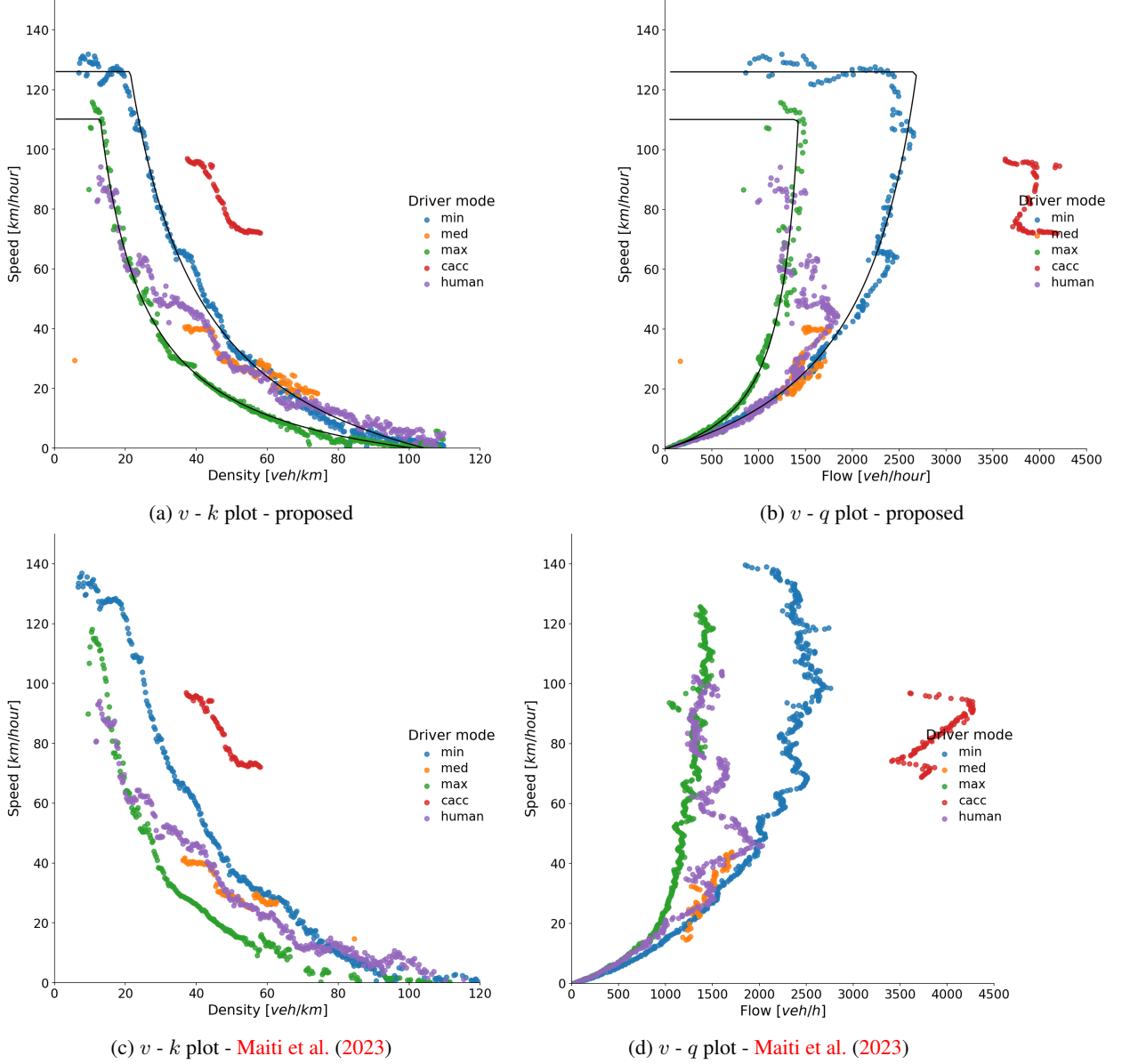


Figure 5: Bi-level plots with the proposed method after aggregation

$$Q_{\S} = \frac{\sqrt{\frac{1}{(M+1)} \sum_{m=0}^M (q_m - Q(k_m))}}{\frac{1}{(M+1)} \sum_{m=0}^M (q_m)} + \frac{\sqrt{\frac{1}{(M+1)} \sum_{m=0}^M (v_m - Q(k_m)/k_m)}}{\frac{1}{(M+1)} \sum_{m=0}^M (v_m)} \quad (11)$$

E Analysis of acceleration, deceleration and stable platoon states

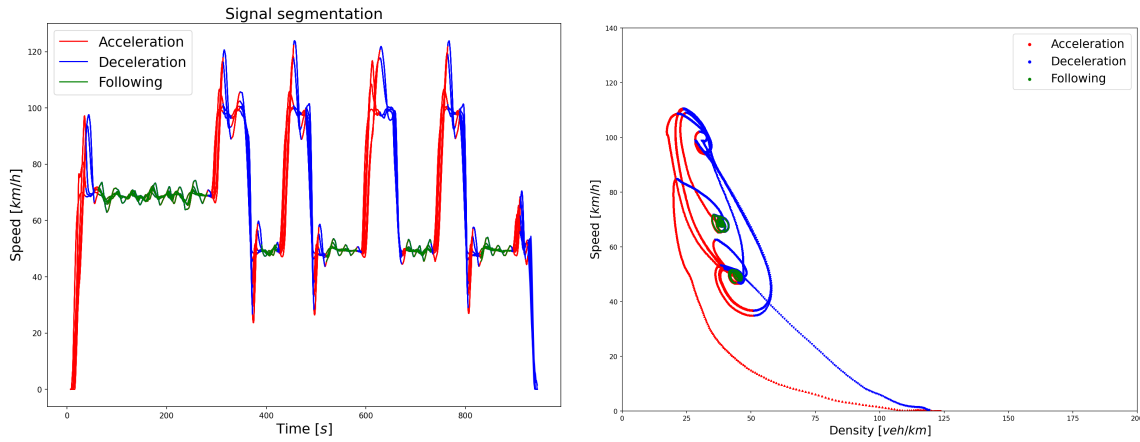
Figure 6a shows the segmented speed profiles from a five-vehicle platoon from the *AstaZero* campaign. The segmentation was performed on the basis of the average platoon speed (platoon profile). We obtain acceleration and deceleration parts using a local min/max algorithm on the platoon profile¹. Furthermore, we manually label the stable parts, that is, partial speed profiles where the vehicles follow each other in platoon formation with only slight speed variations.

¹<https://www.csc.kth.se/weinkauf/notes/persistence1d.html>

Figure 6b shows the speed-density ($v-k$) plot as they are computed by Eq. 3a and Eq. 3c respectively, for the platoon measurements shown in Figure 6a. The colors correspond to the three different states mentioned above. Noticing the green points that correspond to equilibrium conditions, it is already visible a quasi-linear relation between platoon production and platoon density, (similar to the speed-spacing relation in the analysis of trajectories at link level). The speed-density and flow-speed plots are shown for completion in Figure 7.

F Sensitivity analysis on the aggregation process

The calibration results for different δ values are summarized in Table 2. It is interesting to observe that the calibrated TFD parameters for the minimum and maximum δ s remain consistent, even for higher δ values, that normally lead to very few points for calibration. A visual illustration of the $q - k$ plot for different δ values is shown in Figure 8.



(a) Speed profile segmentation based on platoon average speed in acceleration, deceleration and following state events. (b) The derived $v - k$ diagram for a partial platoon trajectory from the *AstaZero* campaign.

Figure 6: Acceleration, deceleration and stable platoon states.

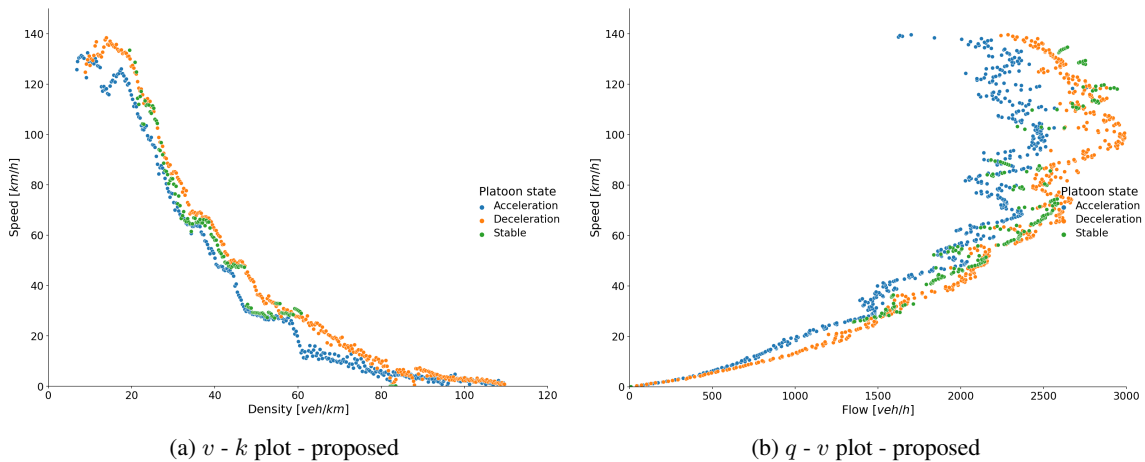
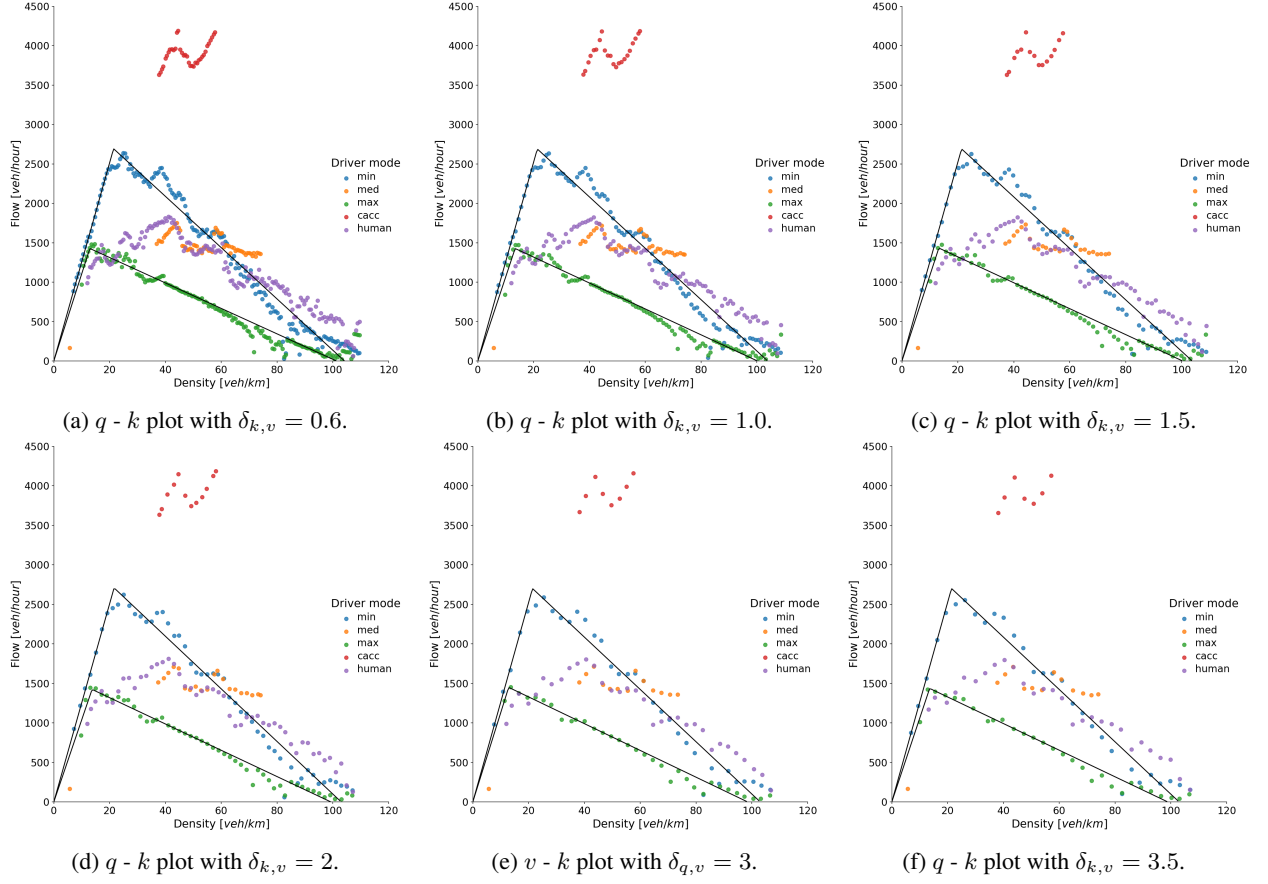


Figure 7: Bi-level plots for different platoon states. The plots refer to observed vehicle platoons driven with the ACC minimum setting.

Figure 8: Sensitivity analysis for the consistency of the calibrated $q - k$ plots of the FD for 6 additional $\delta_{k,v}$ values.Table 2: Calibrated TFD parameters that remain consistent for different $\delta_{k,v}$ values.

$\delta_{k,v}$	setting	$v_f [km/h]$	$k_{cr} [veh/km]$	$k_{jam} [veh/km]$	$w [km/h]$
0.3	<i>min</i>	126.0	21.3	104.4	32.4
0.3	<i>max</i>	110.1	12.9	101.0	16.2
0.6	<i>min</i>	125.8	21.4	104.2	32.5
0.6	<i>max</i>	110.6	12.9	101.3	16.2
1.0	<i>min</i>	126.2	21.3	103.9	32.6
1.0	<i>max</i>	106.8	13.4	100.2	16.4
1.5	<i>min</i>	126.2	21.3	103.8	32.6
1.5	<i>max</i>	108.7	13.2	100.3	16.4
2	<i>min</i>	125.4	21.6	103.0	33.3
2	<i>max</i>	104.0	13.7	99.2	16.6
3	<i>min</i>	126.2	21.4	103.0	33.1
3	<i>max</i>	112.9	12.8	98.5	16.9
3.5	<i>min</i>	126.2	21.4	103.0	33.1
3.5	<i>max</i>	106.0	13.6	98.9	16.8

References

- Apostolakis, T., Makridis, M.A., Kouvelas, A., Ampountolas, K., 2023. Energy-Based Assessment and Driving Behavior of ACC Systems and Humans Inside Platoons. *IEEE Transactions on Intelligent Transportation Systems* , 1–10doi:doi:10.1109/TITS.2023.3285296. conference Name: IEEE Transactions on Intelligent Transportation Systems.
- van Arem, B., van Driel, C.J.G., Visser, R., 2006. The Impact of Cooperative Adaptive Cruise Control on Traffic-Flow Characteristics. *IEEE Transactions on Intelligent Transportation Systems* 7, 429–436. doi:doi:10.1109/TITS.2006.884615. conference Name: IEEE Transactions on Intelligent Transportation Systems.
- Brunner, J.S., Makridis, M.A., Kouvelas, A., 2022. Comparing the Observable Response Times of ACC and CACC Systems. *IEEE Transactions on Intelligent Transportation Systems* , 1–10doi:doi:10.1109/TITS.2022.3165648. conference Name: IEEE Transactions on Intelligent Transportation Systems.
- Cassidy, M.J., Coifman, B., 1997. Relation Among Average Speed, Flow, and Density and Analogous Relation Between Density and Occupancy. *Transportation Research Record* 1591, 1–6. URL: <https://doi.org/10.3141/1591-01>, doi:doi:10.3141/1591-01. publisher: SAGE Publications Inc.
- Chen, D., Ahn, S., Chitturi, M., Noyce, D.A., 2017. Towards vehicle automation: Roadway capacity formulation for traffic mixed with regular and automated vehicles. *Transportation Research Part B: Methodological* 100, 196–221. URL: <https://www.sciencedirect.com/science/article/pii/S0191261516305471>, doi:doi:10.1016/j.trb.2017.01.017.
- Daganzo, C.F., 1995. Requiem for second-order fluid approximations of traffic flow. *Transportation Research Part B: Methodological* 29, 277–286. URL: <https://www.sciencedirect.com/science/article/pii/S019126159500007Z>, doi:doi:10.1016/0191-2615(95)00007-Z.
- Du, Y., Makridis, M.A., Tampère, C.M.J., Kouvelas, A., ShangGuan, W., 2023. Adaptive control with moving actuators at motorway bottlenecks with connected and automated vehicles. *Transportation Research Part C: Emerging Technologies* 156, 104319. URL: <https://www.sciencedirect.com/science/article/pii/S0968090X2300308X>, doi:doi:10.1016/j.trc.2023.104319.
- Edie, L.C., 1965. Discussion of traffic stream measurements and definitions. *Proceedings of the Second International Symposium on the Theory of Traffic Flow, London 1963.* , 139–154OCLC: 291099209.
- Gunter, G., Gloudemans, D., Stern, R.E., McQuade, S., Bhadani, R., Bunting, M., Delle Monache, M.L., Lysecky, R., Seibold, B., Sprinkle, J., Piccoli, B., Work, D.B., 2021. Are Commercially Implemented Adaptive Cruise Control Systems String Stable? *IEEE Transactions on Intelligent Transportation Systems* 22, 6992–7003. doi:doi:10.1109/TITS.2020.3000682.
- He, Y., Makridis, M., Fontaras, G., Mattas, K., Xu, H., Ciuffo, B., 2020. The energy impact of adaptive cruise control in real-world highway multiple-car-following scenarios. *European Transport Research Review* 12, 17. URL: <https://doi.org/10.1186/s12544-020-00406-w>, doi:doi:10.1186/s12544-020-00406-w.
- Ioannou, P.A. (Ed.), 1997. *Automated Highway Systems*. Springer US, Boston, MA. URL: <http://link.springer.com/10.1007/978-1-4757-4573-3>, doi:doi:10.1007/978-1-4757-4573-3.
- Kouvelas, A., Saeedmanesh, M., Geroliminis, N., 2017. Enhancing model-based feedback perimeter control with data-driven online adaptive optimization. *Transportation Research Part B: Methodological* 96, 26–45. URL: <http://www.sciencedirect.com/science/article/pii/S019126151630710X>, doi:doi:10.1016/j.trb.2016.10.011.
- Laval, J.A., 2011. Hysteresis in traffic flow revisited: An improved measurement method. *Transportation Research Part B: Methodological* 45, 385–391. URL: <https://www.sciencedirect.com/science/article/pii/S0191261510001013>, doi:doi:10.1016/j.trb.2010.07.006.
- Li, T., Chen, D., Zhou, H., Laval, J., Xie, Y., 2021. Car-following behavior characteristics of adaptive cruise control vehicles based on empirical experiments. *Transportation Research Part B: Methodological* 147, 67–91. URL: <https://www.sciencedirect.com/science/article/pii/S0191261521000424>, doi:doi:10.1016/j.trb.2021.03.003.
- Lu, Q.L., Yang, K., Antoniou, C., 2021. Crash risk analysis for the mixed traffic flow with human-driven and connected and autonomous vehicles, in: *2021 IEEE International Intelligent Transportation Systems Conference (ITSC)*, pp. 1233–1238. doi:doi:10.1109/ITSC48978.2021.9564897.
- Ma, K., Wang, H., Ruan, T., 2021. Analysis of road capacity and pollutant emissions: Impacts of Connected and automated vehicle platoons on traffic flow. *Physica A: Statistical Mechanics and its Applications* 583, 126301. URL: <https://www.sciencedirect.com/science/article/pii/S0378437121005744>, doi:doi:10.1016/j.physa.2021.126301.

- Maiti, N., Laval, J., Chilukuri, B.R., 2023. Universality of Area Occupancy-Based Fundamental Diagrams in Mixed Traffic. URL: <https://papers.ssrn.com/abstract=4474351>, doi:doi:10.2139/ssrn.4474351.
- Makridis, M., Leclercq, L., Ciuffo, B., Fontaras, G., Mattas, K., 2020a. Formalizing the heterogeneity of the vehicle-driver system to reproduce traffic oscillations. *Transportation Research Part C: Emerging Technologies* 120, 102803. Publisher: Pergamon.
- Makridis, M., Mattas, K., Anesiadou, A., Ciuffo, B., 2020b. Open ACC Database. European Commission, Joint Research Centre -. URL: <http://data.europa.eu/89h/9702c950-c80f-4d2f-982f-44d06ea0009f>.
- Makridis, M., Mattas, K., Anesiadou, A., Ciuffo, B., 2021. OpenACC. An open database of car-following experiments to study the properties of commercial ACC systems. *Transportation Research Part C: Emerging Technologies* 125, 103047. URL: <https://www.sciencedirect.com/science/article/pii/S0968090X21000772>, doi:doi:10.1016/j.trc.2021.103047.
- Makridis, M., Mattas, K., Ciuffo, B., 2020c. Response Time and Time Headway of an Adaptive Cruise Control. An Empirical Characterization and Potential Impacts on Road Capacity. *IEEE Transactions on Intelligent Transportation Systems* 21, 1677–1686. URL: <https://ieeexplore.ieee.org/document/8884686>, doi:doi:10.1109/TITS.2019.2948646.
- Makridis, M., Mattas, K., Mogno, C., Ciuffo, B., Fontaras, G., 2020d. The impact of automation and connectivity on traffic flow and CO2 emissions. A detailed microsimulation study. *Atmospheric Environment* 226, 117399. URL: <http://www.sciencedirect.com/science/article/pii/S1352231020301382>, doi:doi:10.1016/j.atmosenv.2020.117399.
- Makridis, M.A., Kouvelas, A., 2023. An adaptive framework for real-time freeway traffic estimation in the presence of CAVs. *Transportation Research Part C: Emerging Technologies* 149, 104066. URL: <https://www.sciencedirect.com/science/article/pii/S0968090X23000554>, doi:doi:10.1016/j.trc.2023.104066.
- Mattas, K., Makridis, M., Botzoris, G., Kriston, A., Minarini, F., Papadopoulos, B., Re, F., Rognelund, G., Ciuffo, B., 2020. Fuzzy Surrogate Safety Metrics for real-time assessment of rear-end collision risk. A study based on empirical observations. *Accident Analysis & Prevention* 148, 105794. URL: <https://www.sciencedirect.com/science/article/pii/S0001457520316146>, doi:doi:10.1016/j.aap.2020.105794.
- Mullakkal-Babu, F.A., Wang, M., He, X., van Arem, B., Happee, R., 2020. Probabilistic field approach for motorway driving risk assessment. *Transportation Research Part C: Emerging Technologies* 118, 102716. URL: <https://www.sciencedirect.com/science/article/pii/S0968090X20306318>, doi:doi:10.1016/j.trc.2020.102716.
- Shi, X., Li, X., 2021. Constructing a fundamental diagram for traffic flow with automated vehicles: Methodology and demonstration. *Transportation Research Part B: Methodological* 150, 279–292. URL: <https://www.sciencedirect.com/science/article/pii/S0191261521001235>, doi:doi:10.1016/j.trb.2021.06.011.
- Tiernan, T., Bujanovic, P., Azeredo, P., Najm, W.G., Lochrane, T., 2019. CARMA Testing and Evaluation of Research Mobility Applications. Federal Highway Administration, U.S. DoT URL: <https://ntl.bts.gov/public-access>, doi:doi:10.21949/1503647. publisher: Not Available.
- Tiernan, T.A., Richardson, N., Azeredo, P., Najm, W.G., Lochrane, T., 2017. Test and Evaluation of Vehicle Platooning Proof-of-Concept Based on Cooperative Adaptive Cruise Control. Federal Highway Administration, U.S. DoT URL: <https://ntl.bts.gov/public-access>, doi:doi:10.21949/1503647. publisher: Not Available.
- Treiterer, J., 1975. Investigation of traffic dynamics by aerial photogrammetry techniques. Engineering Experiment Station, Ohio State University. URL: <https://trid.trb.org/view/30152>. number: EES-278 Final Rpt.
- Treiterer, J., Myers, J.A., 1974. The hysteresis phenomenon in traffic flow, in: *Proceedings of the 6th International Symposium on Transportation and Traffic Theory held at the University of New South Wales, Sydney, Australia from 26-28 August 1974.*, pp. 13–38. URL: <https://trid.trb.org/view/40314>.
- Xu, D., Xue, C., Zhou, H., 2021. Analysis of Headway and Speed Based on Driver Characteristics and Work Zone Configurations Using Naturalistic Driving Study Data. *Transportation Research Record* 2675, 1196–1210. URL: <https://doi.org/10.1177/03611981211015261>, doi:doi:10.1177/03611981211015261. publisher: SAGE Publications Inc.